Elastodynamic models for extending GTD to penumbra and finite size flaws

A.K. Djakou, Michel Darmon, Catherine Potel

Journal of Physics: Conference Series **684** (2016) 012002 doi:10.1088/1742-6596/684/1/012002

Elastodynamic models for extending GTD topenumbra and finite size flaws

A Kamta Djakou[1], M Darmon[1] and C Potel[2,3]

[1] CEA, LIST, F91191 Gif-sur-Yvette, France
[2] LAUM, UMR CNRS 6613, 72085 Le Mans cedex 9, France
[3] Fédération Acoustique du Nord Ouest (FANO), FR CNRS 3110, France

E-mail: audrey.kamta-djakou@cea.fr

Abstract. The scattering of elastic waves from an obstacle is of great interest in ultrasonic Non Destructive Evaluation (NDE). There exist two main scattering phenomena: specular reflection and diffraction. This paper is especially focused on possible improvements of the Geometrical Theory of Diffraction (GTD), one classical method used for modelling diffraction from scatterer edges. GTD notably presents two important drawbacks: it is theoretically valid for a canonical infinite edge and not for a finite one and presents discontinuities around the direction of specular reflection. In order to address the first drawback, a 3D hybrid method using both GTD and Huygens secondary sources has been developed to deal with finite flaws. ITD (Incremental Theory of Diffraction), a method developed in electromagnetism, has also been developed in elastodynamics to deal with small flaws. Experimental validation of these methods has been performed. As to the second drawback, a GTD uniform correction, the UTD (Uniform Theory of Diffraction) has been developed in the view of designing a generic model able to correctly simulate both specular reflection and diffraction. A comparison has been done between UTD numerical results and UAT (Uniform Asymptotic Theory of Diffraction) which is another uniform solution of GTD.

1. Introduction

The scattering of elastic waves by an obstacle is constituted of phenomena such as the specular reflection and the diffraction. The simplest way to model scattering is the strong approximation of the Geometrical Elastodynamics (GE) which just considers incident and reflected waves. This approximation gives rise to three main regions of space when a plane wave interacts with a crack half-plane: the region illuminated by both incident and reflected waves, the region illuminated only by the incident waves and the shadow region where there is no wave. These regions (see Fig. 1) are separated by shadow boundaries (SB), the incident and reflected shadow boundaries. GE predicts a discontinuity of the elastodynamic field when crossing these shadow boundaries.

This discontinuity of the geometrical field comes from the fact that diffracted waves by the crack edge are not taken into account in GE. There exist a number of methods to model diffraction as the Kirchoff Approximation(KA) [1, 2] and the Geometrical Theory of Diffraction (GTD) [2, 3, 4]. They are all high frequency methods and thus own some limitations. For instance the quantitative prediction by KA of edge diffraction can be erroneous notably for SV waves [5]. Numerical methods as finite elements or finite differences are also used to model the scattering problem. They are time consuming and are generally used for inspection of component or flaws with complex geometry.

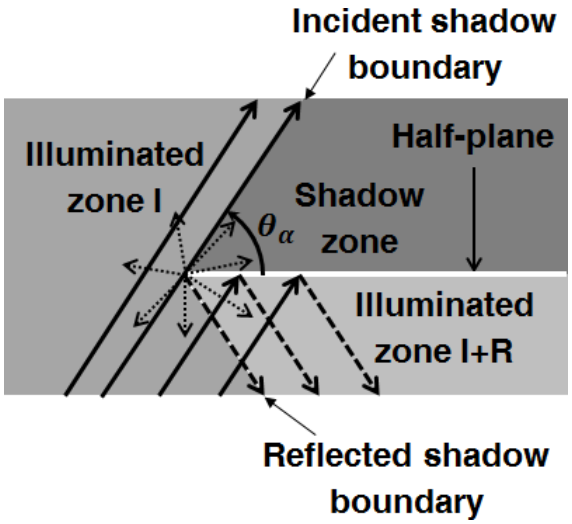

Figure 1: Scattering of a plane wave by a semi-infinite crack embedded in an elastic homogeneous solid. Thick arrows - incident waves, dash arrows - reflected waves, dotted arrows - diffracted waves.

GTD is an extension of GE. Indeed, it adds diffracted rays to incident and reflected rays. These diffracted rays propagate in shadow regions whereby the classical geometrical rays could not (see Fig. 1). The GTD diffracted field is the product of the incident field weighted by a diffraction coefficient and a divergence factor. The phase function of the diffracted field respects the eikonal equation and the divergence factor ensures the energy conservation in a tube of rays. The diffraction coefficient is obtained thanks to canonical configurations as half-planes or wedges. Therefore, GTD does not take into account the finite length of the diffracting edges encountered in NDE. Furthermore, GTD fails in the zones where edge diffracted waves interfere with incident or reflected waves. For this reason, GTD solution is said to be non-uniform.

To overcome these shortcomings of GTD, in a first step, points on the diffracting edge are considered as fictive sources of a field called incremental field. This approach of the problem is called incremental method. Incremental methods have been principally developed in electromagnetism: Incremental Theory of Diffraction (ITD) [6, 7, 8], Incremental Length Diffraction Coefficient (ILDC) [9] and Equivalent Edge Currents (EEC) [10]. They have also been developed in acoustics [11, 12, 13]. In this paper, it is shown that ITD can be extended from electromagnetism to elastodynamics and another incremental model based on Huygens' principle has been developed. In a second step, a uniform extension of GTD, the Uniform Theory of Diffraction (UTD) [14, 15] based on the Pauli-Clemmow process [16], has been developed in elastodynamics in the aim to overcome the second GTD drawback (failure at specular direction). UTD is preferred to UAT (Uniform Asymptotic Theory of diffraction) [17, 18], another uniform extension of GTD, because UAT involves artificial extension of the scattering surface and fictitious reflected rays while UTD does not. UTD is also preferred to the Physical Theory of Diffraction (PTD), a correction of KA in diffraction [19, 20, 21], shown to be equivalent to UAT at the first order [22]. PTD can be time consuming for large scatterers since it is an integral method.

This paper focuses on the development of incremental models and of UTD in elastodynamics. The geometry of the problem is first introduced in section 2. Then, in section 3, the two incremental models, ITD and Huygens-based, are developed in elastodynamics and then experimentally validated. In section 4, UAT result is recalled and UTD is developed in

elastodynamics. A numerical comparison between UTD and UAT is performed. Conclusions are provided in section 5.

2. Problem statement

In the following, the symbols α and β are used to denote the wave type, i.e. α, β = L, TV or TH (Longitudinal, Transverse Vertical or Transverse Horizontal, respectively). α is used for the incident wave and β for reflected and diffracted waves. Scalar quantities are labelled by taking α and β as subscripts, while α is used as superscripts for vectors related to the incident wave and β as subscripts for vectors related to scattered waves.

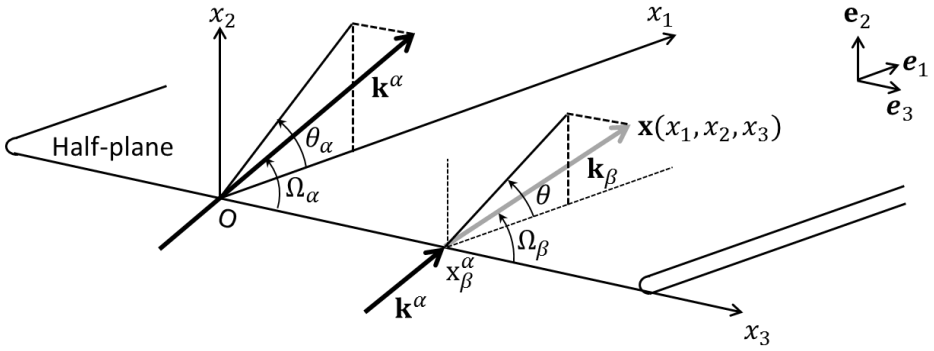

Figure 2: A plane wave of propagation vector $\mathbf{k}^\alpha$ incident on a semi-infinite stress-free crack. Thick black arrow - direction of the incident wave; thick gray arrow - direction of the diffracted wave ($\mathbf{k}_\beta$).

The geometry of the problem is presented in Fig. 2, using the Cartesian system based on an orthonormal basis $\{\mathbf{e}_1, \mathbf{e}_2, \mathbf{e}_3\}$ and the origin O on the crack edge. The crack is embedded in an elastic homogeneous and isotropic space and is the half-plane $\{x_2 = 0, x_1 \geq 0\}$. The edge coincides with the x_3 axis and is irradiated by a plane wave

$$\mathbf{u}^\alpha(\mathbf{x}, \Omega_\alpha, \vartheta_\alpha) = A\, \mathbf{d}^\alpha e^{i(-\omega t + \mathbf{k}^\alpha \cdot \mathbf{x})}, \tag{1}$$

where A is the wave displacement amplitude; $\mathbf{d}^\alpha$ is its polarization; $\mathbf{k}^\alpha$ its wave vector defined thanks to the angles Ω_α and ϑ_α (described in Fig. 2), whose magnitude $k_\alpha = \omega/c_\alpha$, with ω - the angular frequency and c_α - the speed of the corresponding mode; t is time; and $\mathbf{x}$ is the position vector, expressed in the Cartesian coordinates as (x_1, x_2, x_3) and in cylindrical coordinates as (r, ϑ, x_3). The exponential factor $\exp(-i\omega t)$ is implied but omitted everywhere.

The approximate GTD-based total field [4] can be expressed as

$$\mathbf{u}^{\mathrm{tot(GTD)}}(\mathbf{x}, \Omega_\alpha, \vartheta_\alpha) = \mathbf{u}^{\alpha(\mathrm{GE})}(\mathbf{x}, \Omega_\alpha, \vartheta_\alpha) + \sum_\beta \mathbf{u}_\beta^{\alpha(\mathrm{GTD})}(\mathbf{x}, \Omega_\alpha, \vartheta_\alpha), \tag{2}$$

where

$$\mathbf{u}^{\alpha(\mathrm{GE})}(\mathbf{x}, \Omega_\alpha, \vartheta_\alpha) = H(\eta_\alpha)\, \mathbf{u}^\alpha(\mathbf{x}, \Omega_\alpha, \vartheta_\alpha) + \sum_\beta H(\eta_\beta)\, \mathbf{u}_\beta^{\alpha(\mathrm{ref})}(\mathbf{x}, \Omega_\alpha, \vartheta_\alpha), \tag{3}$$

with H being the Heaviside function and

$$\mathbf{u}_\beta^{\alpha(\mathrm{ref})}(\mathbf{x}, \Omega_\alpha, \vartheta_\alpha) = AR^\alpha{}_\beta \mathbf{d}_\beta\, (-q_\beta \cos\vartheta_\beta)\; e^{i k_\beta \mathbf{p}_\beta \cdot \mathbf{x}} \tag{4}$$

the reflected field. In equation (4), $\mathbf{p}_\beta = (\sin\Omega_\beta \cos\vartheta_\beta, -\sin\Omega_\beta \sin\vartheta_\beta, \cos\Omega_\beta)$ is the unit reflected wave vector and $\mathbf{d}_\beta\ (-q_\beta \cos\vartheta_\beta)$ its polarisation vector. The polarisation vector of the reflected field depends on the parameter $q_\beta \cos\vartheta_\beta$ where $q_\beta = k_\beta \sin\Omega_\beta$ and ϑ_β is the reflection angle which is related to the incidence angle ϑ_α by Snell's law

$$q_\beta \cos\vartheta_\beta = q_\alpha \cos\vartheta_\alpha. \tag{5}$$

The diffraction angle Ω_β is related to the incidence angle Ω_α by Snells law in diffraction

$$k_\beta \cos\Omega_\beta = k_\alpha \cos\Omega_\alpha. \tag{6}$$

The arguments $\eta_\alpha = \mathrm{sgn}(\vartheta - \vartheta_\alpha)$ and $\eta_\beta = \mathrm{sgn}(\vartheta - 2\pi + \vartheta_\beta)$ of the respective Heaviside functions determine whether the observation point is in the illuminated region or shadow of incident and reflected waves (see Fig. 1). The GTD diffracted field [4] is expressed as

$$\mathbf{u}_\beta^{\alpha(\mathrm{GTD})}(\mathbf{x}, \Omega_\alpha, \vartheta_\alpha) = u^\alpha(x_\beta^\alpha) D_\beta^{\alpha(\mathrm{GTD})}(\vartheta, \Omega_\alpha, \vartheta_\alpha)\, \mathbf{d}_\beta\,(-q_\beta \cos\vartheta) \frac{e^{ik_\beta S_\beta}}{\sqrt{k_\beta L_\beta}}, \tag{7}$$

where $u^\alpha(x_\beta^\alpha) = \mathbf{u}^\alpha(\mathbf{x}^\alpha)_\beta \cdot \mathbf{d}^\alpha$, $x^\alpha(0, 0, x_3 - S_\beta \cos\Omega_\beta)$ is the diffraction point on the scattering edge (see Fig. 2); $D_\beta^{\alpha(\mathrm{GTD})}$ is the so-called diffraction coefficient; S_β is the distance between the diffraction point $\mathbf{x}_\beta^\alpha$ and the observation point $\mathbf{x}$; $L_\beta = S_\beta \sin^2\Omega_\beta$ is a distance parameter and $\mathbf{d}_\beta\ (-q_\beta \cos\vartheta)$ is the diffracted polarisation vector. In (7), $k_\beta L_\beta$ is the far field parameter. GTD diffraction coefficients contain poles $\vartheta = \vartheta_\beta$ and $\vartheta = 2\pi - \vartheta_\beta$. These poles correspond respectively to the directions of incident and reflected shadow boundaries (see Fig. 1). GTD solution thus diverges at shadow boundaries and is obtained for canonical configurations such as the half-plane in this case. It does not take into account the finite length of the obstacle.

3. Incremental methods

At the diffraction point x_β^α any crack of contour L is locally approximated by a canonical form, a half-plane in this case (see Fig. 3). This half-plane is tangent to the crack at the diffraction point. The diffraction point x_β^α is the origin of the orthonormal basis vector $\{\mathbf{e}_1, \mathbf{e}_2, \mathbf{e}_3\}$ associated to the half-plane. In this localised basis, (S, φ, ϑ) are the spherical coordinates of the observation vector $\mathbf{x}$.

Incremental methods assume that points of the diffracting edge are virtual sources of a field defined as the incremental field $\mathbf{F}_\beta(x_\beta^\alpha, \mathbf{x})$. Thus, the field diffracted by the contour L at an observation point is the integral of the incremental field on the contour L:

$$\mathbf{u}_\beta^\alpha(\mathbf{x}, \Omega_\alpha, \vartheta_\alpha) = \int_L \mathbf{F}_\beta(x_\beta^\alpha, \mathbf{x})\, \mathrm{d}l, \tag{8}$$

with dl being the edge increment. We have developed two different methods in elastodynamics to determine this incremental field: one based on the GTD locality principle (ITD) and one based on the Huygens principle.

3.1. ITD in elastodynamics

ITD is based on the locality principle. It has been developed in electromagnetism [6] and has been extended in elastodynamics in [23]. The ITD incremental field is

$$\mathbf{F}_\beta(x_\beta^\alpha, \mathbf{x}) = \frac{u^\alpha(x_\beta^\alpha)}{\sqrt{2i\pi}} \sin\varphi\, D_\beta^{\alpha(\mathrm{GTD})}(\vartheta, \Omega_\alpha(\varphi), \vartheta_\alpha) \frac{e^{ik_\beta S}}{S} \mathbf{d}_\beta\,(-q_\beta \cos\vartheta), \tag{9}$$

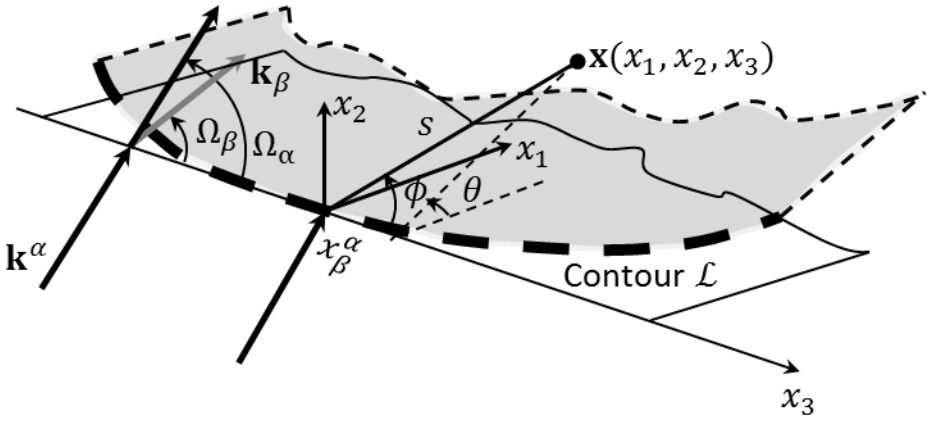

Figure 3: A plane wave of propagation vector $\mathbf{k}^\alpha$ incident on a stress-free obstacle (in gray) of contour LThick black arrow - direction of the incident wave; thick gray arrow - direction of the wave $\mathbf{k}_\beta$ scattered by the half-plane tangent to the crack edge at the flash point x_β^α.

where

$$\Omega_\alpha(\varphi) = \arccos\left(\frac{k_\beta}{k_\alpha}\cos\varphi\right). \tag{10}$$

This incremental field, valid in the far field zone $k_\beta S \gg 1$, is a spherical wave weighted by a coefficient. Therefore, the contour points act as fictive source of spherical waves. It has been checked that ITD gives back GTD solution in the case of the plane wave scattering from a half-plane i.e. for an infinite straight edge. Another incremental model based on the Huygens principle is developed in next section.

3.2. Huygens method

The second method is based on the Huygens principle. It also supposes that points on the diffracting edge are fictive sources of spherical waves which interfere between each other and give rise to the displacement field at an observation point. An Ansatz is proposed so that each spherical wave is weighted by a diffraction coefficient proportional to GTD diffraction coefficient $D_\beta^{\alpha(\mathrm{GTD})}$. The diffracted field can therefore be written as

$$\mathbf{u}_\beta^\alpha(\mathbf{x}, \Omega_\alpha, \vartheta_\alpha) = \int_L \mathrm{C}\, u^\alpha(x_\beta^\alpha) D_\beta^{\alpha(\mathrm{GTD})}(\vartheta, \Omega_\alpha, \vartheta_\alpha) \frac{e^{ik_\beta S}}{S} \mathbf{d}_\beta(-q_\beta\cos\vartheta)\,\mathrm{d}l \tag{11}$$

where L is the crack contour; C is an unknown parameter to determine and dl is the edge increment. To find the value of the parameter C, the stationary phase method is applied to (11) in the case of a straight infinite edge and equalized to (7) because the contribution of the stationary point corresponds to the edge diffracted field. Finally,

$$\mathrm{C} = \frac{\sin\Omega_\beta}{\sqrt{2i\pi}}. \tag{12}$$

The incremental fields ITD and Huygens-based are respectively

$$\mathbf{F}_\beta(x_\beta^\alpha, \mathbf{x})\cdot_{\mathrm{ITD}} = u^\alpha(x_\beta^\alpha) K(\varphi(l)) \frac{e^{ik_\beta S}}{S} \mathbf{d}_\beta(-q_\beta\cos\vartheta), \tag{13}$$

$$\mathbf{F}_\beta(x_\beta^\alpha, \mathbf{x})\cdot_{\mathrm{Huygens}} = u^\alpha(x_\beta^\alpha) K(\Omega_\beta) \frac{e^{ik_\beta S}}{S} \mathbf{d}_\beta(-q_\beta\cos\vartheta), \tag{14}$$

with the coefficient

$$K(\zeta) = \frac{\sin\zeta}{\sqrt{2i\pi}} D_{\beta}^{\alpha(\mathrm{GTD})}(\vartheta, \Omega_{\alpha}(\zeta), \vartheta_{\alpha}). \quad (15)$$

Huygens method (14) differs from ITD (13) in the case of a straight edge only by the argument ζ of the coefficient $K(\zeta)$. For Huygens, this argument ζ is the diffraction angle Ω_{β} linked to the incidence angle Ω_{α} by Snell-J's law of diffraction (6) whereas for ITD it is the angle φ between the observation point and the discretization point (see Fig. 3). These incremental models can be applied to GTD and also to uniform GTD corrections. They have been validated experimentally in the following.

3.3. Experimental validation

Diffracted echoes generated by the top tip of a 40 mm large and 10 mm high backwall breaking planar notch simulated by incremental methods are compared to experimental results for various flaw orientations with respect to the probes one.

Diffraction echoes have been measured in the TOFD (Time Of Flight Diffraction) inspection of a ferritic steel component (see Fig. 4) using two 6.35 mm diameter mono-element probes emitting P45 waves at 2.25 MHz with a 60 mm PCS (Probe Centre Spacing). This ferritic steel component is defined in the Cartesian coordinates (X, Y, Z) shown in Fig. 4. The defect is initially perpendicular to X-axis so that it is inspected in a 2D configuration. Then, the skew angle (angle between the flaw top edge and the Y-axis) is increased from 0°(2D configuration) to 70°(see Fig. 4) in order to be in a 3D configuration by rotating the specimen around the Z-axis. The echo generated by a 2 mm diameter and 40 mm length side-drilled hole (see Fig. 4) is employed for calibration.

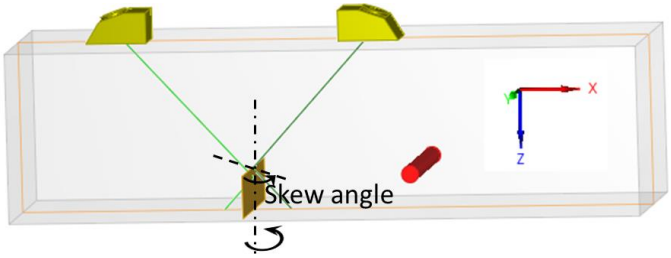

Figure 4: TOFD simulation configuration.

The measured and simulated results are presented in Table 1. ITD and Huygens lead to the same results. The errors between ITD/Huygens simulations and experimental results are at most or around 1dB and are less than the measurements incertitudes (around 2dB).

4. Uniform corrections of GTD in elastodynamics

The classical edge-diffracted GTD ray field is not valid near and at shadow boundaries (directions of specular reflection and direct transmission). Indeed GTD evaluates asymptotically the exact solution of the scattering from a half-plane which is a Sommerfeld integral [24, Ch. 3] and just takes into account the contribution of the integral stationary phase point. This contribution corresponds to the diffracted field whereas the integrand's poles contribution gives rise to the geometrical field. To handle the coalescence of stationary phase points and integrand's poles, interference of diffracted waves with incident and reflected waves of GE, other methods of approximation are used such as the Van Der Waerden's one which gives rise to UAT and the Pauli-Clemmow's one which leads rise to UTD. UAT has already been derived in elastodynamics by [4, 18].

Table 1: Amplitude of diffracted waves in dB.

Skew angle (°)	experiments	ITD	Huygens
0	-13.1	-12.9	-12.9
10	-12.6	-13.0	-13.0
20	-14.2	-13.1	-13.1
30	-13.3	-13.3	-13.3
40	-13.7	-13.7	-13.7
50	-13.6	-14.3	-14.3
60	-14.0	-15.2	-15.2
70	-14.4	-16.3	-16.2

4.1. UAT

The approximate UAT-based total field [4, 17, 18] can be expressed as

$$\mathbf{u}^{\mathrm{tot(UAT)}}(\mathbf{x}) = A \left[\overline{F}(\xi_\alpha) - \hat{\overline{F}}(\xi_\alpha) \right] e^{i\mathbf{k}^\alpha \cdot \mathbf{x}} \mathbf{d}^\alpha + \sum_\beta A R_\beta^\alpha \left[\overline{F}(\xi_\beta) - \hat{\overline{F}}(\xi_\beta) \right] e^{ik_\beta \mathbf{p}_\beta \cdot \mathbf{x}} \mathbf{d}_\beta (q_\beta \cos\vartheta_\beta) \quad (16)$$

$$+ \sum_\beta u^\alpha(\mathbf{x}_\beta^\alpha) D_\beta^{\alpha(GTD)} \frac{e^{ik_\beta S_\beta}}{\sqrt{k_\beta L_\beta}} \mathbf{d}_\beta (q_\beta \cos\vartheta), \quad (17)$$

where

$$\hat{\overline{F}}(X) = e^{i\frac{\pi}{4}} \frac{e^{iX^2}}{2X\sqrt{\pi}}, \quad (18)$$

$$F(X) = \frac{1}{\sqrt{i\pi}} \int_X^{+\infty} e^{it^2} dt \quad (19)$$

is the Fresnel function and the parameters

$$\xi_\alpha = -\mathrm{sgn}(\vartheta - \vartheta_\alpha) \sqrt{2k_\alpha L_\alpha \sin^2 \frac{\vartheta_\alpha - \vartheta}{2}} \quad (20)$$

$$\text{and} \quad \xi_\beta = -\mathrm{sgn}(\vartheta + \vartheta_\beta - 2\pi) \sqrt{2k_\beta L_\beta \sin^2 \frac{\vartheta_\beta + \vartheta}{2}} \quad (21)$$

are the detour parameters [17]. The divergence of GTD near shadow boundaries is removed by the function $\hat{\overline{F}}$. The asymptotic development of the Fresnel function for large arguments [25] is

$$\overline{F}(X) \simeq H(-X) + \hat{\overline{F}}(X). \quad (22)$$

Then, far away of the shadow boundaries, UAT total field (16) gives back GTD total field (2). In this UAT solution, the incident and reflected field are no more defined only in illuminated regions. They are defined on the whole space. Indeed, UAT needs to extend reflected rays in the shadow region by introducing fictitious rays [26].

4.2. UTD

The approximate UTD-based total field [27] can be expressed as

$$\mathbf{u}^{\mathrm{tot(UTD)}}(\mathbf{x}, \Omega_\alpha, \vartheta_\alpha) = \mathbf{u}_\beta^{\alpha(\mathrm{GE})}(\mathbf{x}, \Omega_\alpha, \vartheta_\alpha) + \sum_\beta F(k_\beta L_\beta\, a)\, \mathbf{u}_\beta^{\alpha(\mathrm{GTD})}(\mathbf{x}, \Omega_\alpha, \vartheta_\alpha), \qquad (23)$$

where F is a transition function and the parameter a describes the proximity of the observation point to a shadow boundary. When the observation point is far away from the shadow boundaries, the transition function tends to 1 and then, UTD is equal to GTD. When the observation point is close to the shadow boundaries, the transition function tends to 0 and removes the singularity of GTD diffraction coefficient; it also introduces a discontinuity in the diffracted field at the shadow boundaries which is cancelled by the GE one so that the total UTD field is continuous at shadow boundaries contrary to GTD.

The UTD just modified the amplitude of the diffracted rays. It does not require fictitious rays as UAT. It is then more simple to implement. UTD asymptotics do not include all terms of the order $(k_\beta L_\beta)^{-1/2}$ as UAT [26, 28]. A comparison between UAT and UTD is performed in the next section.

4.3. Numerical results

The numerical results are presented in the ($\mathbf{e}_1$, $\mathbf{e}_2$) plane, which is perpendicular to the edge crack, since the problem is invariant along the x_3 direction (see Fig. 2). The observation vector $\mathbf{x}$ is specified using the cylindrical coordinates (r, ϑ) associated with the ($\mathbf{e}_1$, $\mathbf{e}_2$) plane. The solid material used for simulations is ferritic steel with Poisson's ratio ν = 0.29, longitudinal velocity c_L = 5900 m.s^{-1} and transversal velocity c_T = 3230 m.s^{-1}.

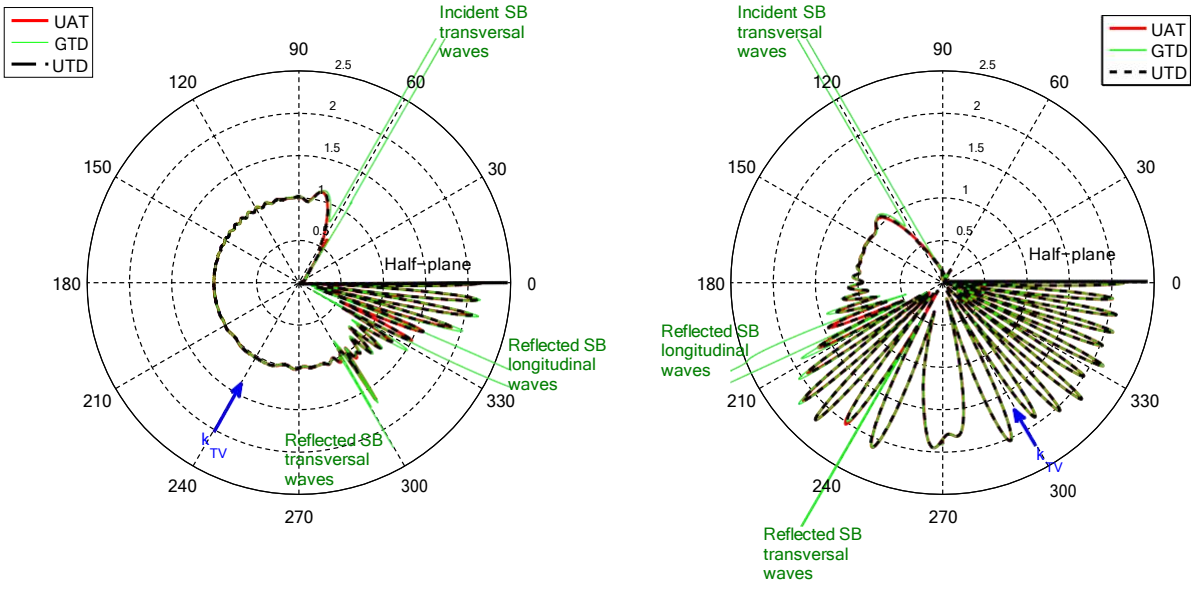

Figure 5: Directivity pattern of the total field predicted by different models (GTD, UAT and UTD) at $r = 10\lambda$ ($k_\beta L_\beta = 20\pi$, $\beta = TV$) for $\Omega_{TV} = 90^\circ$ - (a) $\vartheta_{TV} = 60^\circ$ - (b) $\vartheta_{TV} = 120^\circ$. Each circle represents amplitude of the total field normalized by the incident amplitude.

In Fig. 5, all approximate total fields are calculated using all scattered modes, with GTD-based non uniform asymptotics given by (2), UAT - by (16), and UTD - by (23). The used

configuration is 2D: the incidence is normal to the edge crack (Ω_α = 90˚). The incident wave is transverse vertical. There are three shadow boundaries in Fig. 5.a, the incident TV shadow boundary ϑ = 60˚, reflected TV shadow boundary ϑ = 300˚ and reflected L shadow boundary $\vartheta \approx$336˚. There also have three shadow boundaries in Fig. 5.b, the incident TV shadow boundary ϑ = 120˚, reflected TV shadow boundary ϑ = 240˚ and reflected L shadow boundary $\vartheta \approx$ 204˚. The peaks near critical angles $\vartheta_c \approx$ 56.8˚ and $2\pi - \vartheta_c \approx$ 303, 2˚ are due to the interference of the diffracted T wave with the corresponding head waves generated by diffraction at the edge (see Fig. 6).

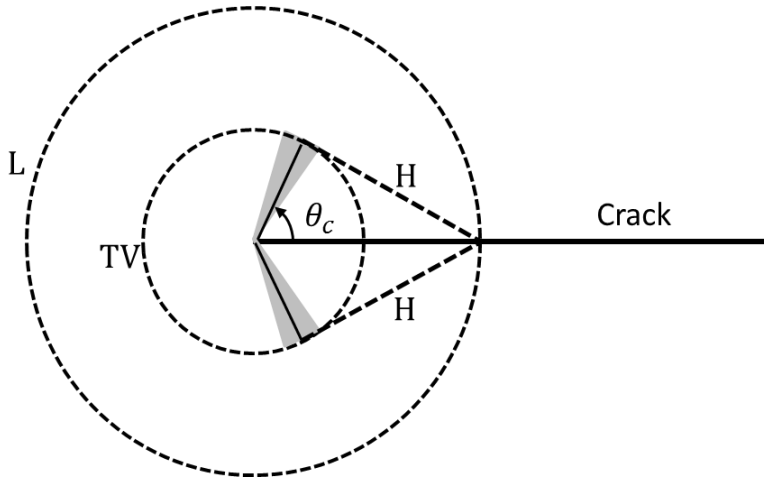

Figure 6: Waves diffracted from a crack edge: L stands for longitudinal wave, TV for transversal and H for head wave; ϑ_c is the longitudinal critical angle.

As expected, both UTD and UAT are continuous at shadow boundaries and practically coincide far away from the shadow boundaries. There is a slight difference between them near the shadow boundaries. In Fig 5.a, there is a difference of peak amplitude at the critical angles between UAT and UTD. That is because, such critical angles are located near the incident and reflected shadow boundaries. In this observation region the diffracted rays (contribution of stationary phase point) interfere with incident or reflected rays (poles) and head waves (branch point). UAT reproduces the peaks of GTD field since it just modifies the geometrical field whereas in UTD, the transition function tends to 0 near shadow boundaries and then reduces the head wave peak amplitude. Nevertheless, both GTD and its uniform corrections are classically not considered to be valid for observation near a critical angle [29]. A modified version of UTD is proposed in [27] so that its prediction is the same as GTD or UAT at critical angle ϑ_c for a longitudinal incident wave.

In Fig 5.b, the poles are far away from the critical angles. In this case, UTD and UAT give approximately the same result far and near shadow boundaries. The maximum error in dB between UTD and UAT is 2dB.

5. Conclusion

This paper focuses on recent advances in modelling the scattering of elastic waves from an obstacle. The GTD ray method, classically used to model edge diffraction, is valid for an infinite edge and not for a finite size scatterer. Moreover, GTD diverges at observation directions of specular reflection and direct transmission (called shadow boundaries). To overcome these limitations of GTD, two incremental models and a GTD uniform correction have been derived in elastodynamics. The two developed ITD and Huygens' models permit to take into account

the finite size of the scatterer edges. These two models give back GTD solution in the case of a straight infinite edge. They have also been both successfully validated experimentally. UTD, a uniform correction of GTD, permits to have a continuous total field. It modifies the amplitude of the diffracted rays near the shadow boundaries in order to remove the GTD divergences and to cancel the discontinuity of the geometrical field. UTD is simpler to implement than UAT which required to build fictitious rays. It gives results close to UAT ones. Incremental methods can be coupled with UTD to build a generic model both spatially uniform and able to deal with finite size flaws.

References

[1] R. K. Chapman, "Ultrasonic scattering from smooth flat cracks: An elastodynamic Kirchhoff diffraction theory," CEGB Report, North Western Region NDT Applications Centre, NWR/SSD/82/0059/R, 1982.
[2] M. Darmon, N. Leymarie, S. Chatillon and S. Mahaut, "Modelling of scattering of ultrasounds by flaws for NDT." Ultrasonic wave propagation in non homogeneous media. Springer Berlin Heidelberg, 61–71 (2009).
[3] J. B. Keller, "Geometrical theory of diffraction," *J. Opt. Soc. Am.* **52**, 116–130 (1962).
[4] J. D. Achenbach, A.K. Gautesen and H. McMaken, *Rays methods for waves in elastic solids* (Pitman, New York, 1982).
[5] M. Darmon, V. Dorval, A. Kamta Djakou, L. Fradkin and S. Chatillon, "A system model for ultrasonic NDT based on the Physical Theory of Diffraction (PTD)," *Ultrasonics*, **64**, 115-127 (2016).
[6] R. Tiberio and S. Maci, "An incremental theory of diffraction: scalar formulation," *IEEE Trans. Ant. Prop.*, **42**, 600–612 (1994).
[7] R. Tiberio, S. Maci and A. Toccafondi, "An incremental theory of diffraction: Electromagnetic formulation," *IEEE Trans. Ant. Prop.*, **43**, 87–96 (1995).
[8] R. Tiberio, A. Toccafondi, A. Polemi and S. Maci, "Incremental theory of diffraction: a new-improved formulation," *IEEE Trans. Ant. Prop.*, **52**, 2234–2243 (2004).
[9] A. D. Yaghjian, "Incremental length diffraction coefficients for arbitrary cylindrical scatterers," *IEEE Trans. Ant. Prop.*, **49**, 1025–1032 (2001).
[10] Y. Z. Umul, "Rigorous expressions for the equivalent edge currents," *Progress in Electromagnetism Research B*, **15**, 77–94 (2009).
[11] U. P. Svensson, R. I. Fred and J. Vanderkooy, "An analytic secondary source model of edge diffraction impulse responses," *J. Acoust. Soc. Am.*, **106**, 2331–2344 (1999).
[12] U. P. Svensson, P. T. Calamia and S. Nakamishi, "Frequency-domain edge diffraction for finite and infinite edges," *Acta. Acust. Acust.*, **95**, 568–572 (2009).
[13] T. K. Stanton, Dezhang Chu and G. V. Norton, "Acoustic diffraction by deformed edges of finite length: theory and experiment," *J. Acoust. Soc. Am.*, **122**, 3167–3176 (2007).
[14] P. H. Pathak and R. G. Kouyoumjian, "The dyadic diffraction coefficient for a perfectly-conducting wedge," DTIC Document, Tech. Rep. (1970).
[15] R. G. Kouyoumjian and P. H. Pathak, "A uniform geometrical theory of diffraction for an edge in a perfectly conducting surface," *Proc. of the IEEE* **62**, 1448–1461 (1974).
[16] P. C. Clemmow, "Some extension to the method of integration by steepest descent," *Quart. Journ. Mech. and Appl. Math.* **III**, 241–256 (1950).
[17] S. W. Lee and G. A. Deschamps, "A uniform asymptotic theory of electromagnetic diffraction by a curved wedge," *IEEE Trans. Ant. Prop.* **24**, 25–34 (1976).
[18] H. McMaken, "A uniform theory of diffraction for elastic solids," *J. Acoust. Soc. Am.* **75**, 1352–1359 (1984).
[19] P. Ya Ufimtsev, *Fundamentals of the physical theory of diffraction* (John Wiley & Sons, New Jersey, 2007).
[20] V. A. Borovikov and B. Y. Kinber, *Geometrical theory of diffraction* (The institution of Electrical Engineers, 1994).
[21] B. Lü, M. Darmon, C. Potel, L. Fradkin and V. Zernov, "Models Comparison for the scattering of an acoustic wave on immersed targets," *J. Phys. Conf. Series* **353**, doi: 10.1088/1742-6596/353/1/012009 (2012).
[22] V. Zernov, L. Fradkin and M. Darmon, "A refinement of the Kirchhoff approximation to the scattered elastic fields". Ultrasonics, **52**, 830–835 (2012).
[23] A. Kamta Djakou, M. Darmon and C. Potel. "Elastodynamic models for extending GTD to finite length defects". Submitted (2015).
[24] V. M. Babich, M. A. Lyalinov and V. E. Grikurov *Diffraction theory, the Sommerfeld-Malyuzhinets technique* (Alpha Sience, 2008), Ch. 3.
[25] V. A. Borovikov, *Uniform stationary phase method* (The institution of Electrical Engineers, 1994).
[26] D. Bouche and F. Molinet, *Méthodes asymptotiques en électromagnétisme*, (Springer-Verlag, 1994).

[27] A. Kamta Djakou, M. Darmon, L. Fradkin and C. Potel, "The Uniform geometrical Theory of Diffraction for elastodynamics: plane wave scattering from a half-plane". To be published in JASA (2015).
[28] F. Molinet, *Acoustic high-frequency diffraction theory*, (Momentum press, New York, 2011).
[29] L. Fradkin, M. Darmon, S. Chatillon and P. Calmon, "A semi-numerical model for the near-critical angle scattering." Submitted (2015).